HAYSTACK OBSERVATIONS OF CS AND CH₃OH TOWARD STAR FORMING REGIONS

E. Jordan,[1] E. Araya,[1] P. Hofner,[1] M. Mateen,[1] and S. Kurtz[2]

RESUMEN

En este artículo se reportan observaciones de la línea $J = 1 \rightarrow 0$ de ^{12}CS en 20 regiones de formación estelar utilizando el telescopio Haystack de 37 m del MIT. También se observaron tres regiones en la línea $J = 1 \rightarrow 0$ de ^{13}CS, y cinco regiones en la transición de 44 GHz de CH₃OH ($J_K = 7_0 \rightarrow 6_1\,A^+$). Las emisiones de ^{13}CS y CH₃OH fueron detectadas en todas las regiones observadas, y la emisión de ^{12}CS fue detectada en 19 de las 20 regiones, 11 de las cuales son nuevas detecciones. Se encontró una alta correlación entre el ancho de la línea de ^{12}CS y la distancia a las regiones, lo que indica que la emisión de ^{12}CS $J = 1 \rightarrow 0$ podría ser utilizada para estimar las distancias a regiones de formación estelar. Asimismo se reporta la detección de variabilidad de los máseres de CH₃OH (44 GHz) en la mayoría de las regiones observadas.

ABSTRACT

We report ^{12}CS $J = 1 \rightarrow 0$ observations toward 20 star forming regions conducted with the MIT 37 m Haystack telescope. Three of the sources were also observed in the ^{13}CS $J = 1 \rightarrow 0$ line, and five sources where observed in the CH₃OH $J_K = 7_0 \rightarrow 6_1\,A^+$ transition at 44 GHz. We detected ^{13}CS and CH₃OH emission toward all sources observed, and ^{12}CS emission toward 19 of the 20 sources in the sample, 11 of which are new detections. We found a strong correlation between the ^{12}CS FWHM and the source distance, indicating the potential use of ^{12}CS $J = 1 \rightarrow 0$ emission as a tool to estimate distances to star forming regions. We also report detection of CH₃OH 44 GHz maser variability in most of the observed sources.

Key Words: H II regions — ISM: molecules — stars: formation

1. INTRODUCTION

The formation of stars takes place in molecular clouds throughout the Galaxy, from nearby low mass star formation at $\sim$100 pc from Earth, to massive star formation that can be studied at distances of several kpc throughout the Galactic plane. The molecular clouds in which star formation occurs are composed of H_2 molecules, He atoms, dust, and a large variety of molecules with much lower abundances than H_2, of which CO is the most abundant ($\sim$$10^{-4}$ with respect to H_2, e.g., Evans 1999).

Observations of interstellar molecules at cm and mm bands have shown to be a powerful astrophysical probe of density, temperature, and other physical parameters of the interstellar medium. Among the most observed molecules are CS and CH₃OH. CS is commonly detected in thermal emission and is a tracer of high density material given its high critical density of more than 10^4 cm^{-3} (e.g., Evans 1999). CH₃OH on the other hand, is well known for its intense maser emission in a variety of transitions (e.g., Menten 1991; Müller, Menten, & Mäder 2004), but a plethora of thermally excited lines has also been observed (see, e.g., Leurini et al. 2007).

In this work we report a small survey conducted with the MIT 37 m Haystack telescope[3] for CS $J = 1 \rightarrow 0$ and CH₃OH $J_K = 7_0 \rightarrow 6_1\,A^+$ emission

---

[1]Physics Department, New Mexico Institute of Mining and Technology, New Mexico, USA.

[2]Centro de Radioastronomía y Astrofísica, Universidad Nacional Autónoma de México, Mexico.

[3]The MIT 37 m Haystack radio telescope is located near Westford, MA. Undergraduate research at the Haystack Observatory of the Northeast Radio Observatory Corporation (NEROC) is supported by a grant from the National Science Foundation.

JORDAN ET AL.

TABLE 1

OBSERVED SOURCES

Source	Pointing position		Distance	Reference
	α(J2000)	δ(J2000)	(kpc)	
S235	05 40 53.25	$+35$ 41 46.9	1.8	(1)
VLA 1623	16 26 26.36	-24 24 30.0	0.15	(2)
IRAS 16293$-$2422	16 32 22.61	-24 28 32.3	0.16	(3)
M8 E	18 04 52.80	-24 26 36.0	1.8	(4)
G9.62+0.19	18 06 14.68	-20 31 31.8	5.7	(5)
G10.47+0.03	18 08 38.22	-19 51 48.7	7.3	(6)
GGD 27	18 19 12.45	-20 47 24.8	1.7	(7)
G20.08$-$0.14	18 28 10.38	-11 28 48.1	4.1	(8)(9)
G28.20$-$0.049	18 42 58.18	-04 13 59.9	9.1	(10)
G31.41+0.31	18 47 34.50	-01 12 43.0	8.5	(6)
IRAS 18566+0408	18 59 09.98	$+04$ 12 35.5	6.7	(11)
W51 e2/e8	19 23 43.91	$+14$ 30 31.4	7.8	(12)
IRAS 20126+4104	20 14 26.02	$+41$ 13 32.0	1.7	(13)
S106 IR	20 27 25.75	$+37$ 22 47.7	1.2	(14)
AFGL 2591	20 29 24.72	$+40$ 11 18.9	1	(15)
MWC 349	20 32 45.45	$+40$ 39 36.8	1.2	(16)
W75N (B)	20 38 36.48	$+42$ 37 33.6	2	(17)
DR21 (OH)	20 38 59.28	$+42$ 22 48.7	3	(12)
IC 1396N	21 40 42.50	$+58$ 16 08.0	0.75	(19)
CEP A East	22 56 18.00	$+62$ 01 49.5	0.73	(20)
NGC 7538S	23 13 44.98	$+61$ 26 49.2	3.5	(21)

REFERENCES: (1) Felli et al. (2004); (2) André, Ward-Thomson, & Barsony (1993); (3) Stark et al. (2004); (4) Shirley et al. (2003); (5) Hofner et al. (1996); (6) Araya et al. (2005a); (7) Martí, Rodríguez, & Reipurth (1995); (8) near kinematic distance from Downes et al. (1980); (9) Wood & Churchwell (1989); (10) Kurtz, Churchwell, & Wood (1994); (11) Araya et al. (2005b); (12) Thronson & Harper (1979); (13) Edris et al. (2005); (14) Noel et al. (2005); (15) Trinidad et al. (2003); (16) Lugo, Lizano, & Garay (2004); (17) Shepherd, Kurtz, & Testi (2004); (18) Campbell et al. (1982); (19) Reipurth et al. (2003); (20) Goetz et al. (1998); (21) Werner et al. (1979).

toward Galactic star forming regions. A subsample of three sources was also observed in the J $= 1 - 0$ transition of ^{13}CS.

2. OBSERVATIONS AND DATA REDUCTION

2.1. *CS Observations*

We observed 20 sources in the ^{12}CS J $= 1 \rightarrow 0$ transition ($\nu_0 = 48.990978$ GHz, Pickett et al. 1998) with the 37 m Haystack telescope, from 2005 April 13 to 22. Three of the sources (M8 E, W75N (B), and DR21 (OH)) were also observed in the ^{13}CS J $= 1 \rightarrow 0$ transition ($\nu_0 = 46.247580$ GHz[4]). The

---

[4]NIST Recommended Rest Frequencies for Observed Interstellar Molecular Microwave Transitions, http://physics.nist.gov/cgi-bin/micro/table5/start.pl

telescope beam widths at 49.0 and 46.2 GHz are approximately $41''$ and $44''$, respectively. The pointing positions and assumed distances to the sources are given in Table 1. The sources are mostly massive star forming regions except for IRAS 16293$-$2422 and VLA 1623 which are low-mass star forming regions, and MWC 349 which is an intermediate mass stellar system with a photo-evaporating disk (Tafoya, Gómez, & Rodríguez 2004).

The observations were conducted with a bandwidth of 17.8 MHz and 8192 channels, giving an initial channel width of 2.17 kHz (0.013 km s^{-1}). We used beam switching with a total on/off cycle of 5 minutes and between 3 to 14 scans were obtained

per source depending on the brightness of the detected lines. The observations were carried out under varying weather conditions. Observations with excessively high system temperatures (i.e., $T_{\mathrm{sys}} > 1000\,\mathrm{K}$) were discarded; for the ^{12}CS observations the data reported in this paper had system temperatures ranging from $470\,\mathrm{K}$ to $940\,\mathrm{K}$ with an average of $\sim 600\,\mathrm{K}$; for the ^{13}CS observations the system temperature ranged from $180\,\mathrm{K}$ to $300\,\mathrm{K}$ with an average value of $\sim 230\,\mathrm{K}$.

2.2. *CH₃OH Observations*

We observed five sources (S235, M8 E, GGD 27, W51 e2/e8, and DR21 (OH)) in the $\mathrm{J}_K = 7_0 \rightarrow 6_1\,\mathrm{A}^+$ methanol (CH₃OH) transition ($\nu_0 = 44.069430\,\mathrm{GHz}$, Pickett et al. 1998). These five sources are known to harbor strong CH₃OH 44 GHz maser emission (e.g., Haschick, Menten, & Baan 1990; Slysh et al. 1994; Kurtz, Hofner, & Vargas 2004), and were observed primarily to obtain pointing corrections for the CS $\mathrm{J} = 1 \rightarrow 0$ observations.

The sources were observed in spectral line mode with a bandwidth of 5.9 MHz, and an initial channel width of $0.72\,\mathrm{kHz}$ ($0.0049\,\mathrm{km\,s^{-1}}$), again using beam switching with a total on/off cycle of 5 minutes. The telescope beam width at this frequency is $\sim 46''$. The system temperatures for the CH₃OH observations ranged from $230\,\mathrm{K}$ to $365\,\mathrm{K}$ with an average value of $\sim 320\,\mathrm{K}$. From the antenna temperature spectra obtained during the observations we determined the LSR velocity of the peak intensity channel and conducted narrow band (0.66 MHz) continuum pointing observations to determine the telescope pointing corrections. Based on the measured pointing corrections, the telescope pointing accuracy was $\sim 12''$ or better.

2.3. *Calibration*

The planet Jupiter was observed several times at each of the frequencies of the three spectral lines (CS $\mathrm{J} = 1 \rightarrow 0$, ^{13}CS $\mathrm{J} = 1 \rightarrow 0$, and CH₃OH 44 GHz). Based on these observations the calibration factors between antenna temperature and main beam brightness temperature for extended sources were 6.9, 6.3 and 6.7 ($T_{\mathrm{MB}}/T_{\mathrm{a}}$) for the CS $\mathrm{J} = 1 \rightarrow 0$, ^{13}CS $\mathrm{J} = 1 \rightarrow 0$, and CH₃OH 44 GHz transitions, respectively. These values were used to calibrate the spectra from antenna temperature to main beam brightness temperature. Maser spectra were calibrated to flux density units using a conversion factor of 3.4 Jy/K. In the case of W51 e2/e8 we found that (excluding clear variability based on changes in

TABLE 2

FINAL CHANNEL WIDTH AND RMS

Source	Molecule	Channel width $(\mathrm{km\,s^{-1}})$	rms (K)
S235	CH₃OH	0.079	1.6
VLA 1623	^{12}CS	0.21	0.17
IRAS 16293-2422	^{12}CS	0.21	1.7
M8 E	^{12}CS	0.21	2.7
	^{13}CS	0.45	0.30
	CH₃OH	0.039	2.7
G9.62+0.19	^{12}CS	0.43	0.79
G10.47+0.03	^{12}CS	0.21	1.3
GGD 27	^{12}CS	0.21	1.9
	CH₃OH	0.079	1.9
G20.08−0.14	^{12}CS	0.43	0.68
G28.20−0.049	^{12}CS	0.43	0.68
G31.41+0.31	^{12}CS	0.85	1.0
IRAS 18566+0408	^{12}CS	0.43	0.42
W51 e2/e8	^{12}CS	0.21	1.7
	CH₃OH	0.039	1.5
IRAS 20126+4104	^{12}CS	0.21	0.95
S106 IR	^{12}CS	0.85	0.96
AFGL 2591	^{12}CS	0.21	1.0
MWC 349	^{12}CS	0.43	1.2
W75N (B)	^{12}CS	0.43	1.0
	^{13}CS	0.45	0.27
DR21 (OH)	^{12}CS	0.21	1.8
	^{13}CS	0.90	0.16
	CH₃OH	0.079	1.1
IC 1396N	^{12}CS	0.43	0.90
CEP A East	^{12}CS	0.21	0.79
NGC 7538S	^{12}CS	0.43	1.2

NOTES: The transitions for the molecules listed in the table are: CH₃OH $\mathrm{J}_K = 7_0 \rightarrow 6_1\,\mathrm{A}^+$, ^{12}CS $\mathrm{J} = 1 \rightarrow 0$, and ^{13}CS $\mathrm{J} = 1 \rightarrow 0$.

the line profile) the main beam brightness temperature value of the CH₃OH peak maser is quite consistent (within $\sim 20\%$) with previous observations (see § 4.4).

All data reductions and calibrations were done using CLASS[5]. After calibration the spectra were averaged, baselines were subtracted using polynomial fits, and smoothed to the channel width reported in Table 2, where we also report the final rms noise in the spectra. Tables 3, 4, and 5 list the line parameters of the ^{12}CS, ^{13}CS, and CH₃OH 44 GHz observations, respectively.

3. RESULTS

In Figures 1 and 2 we show the ^{12}CS $\mathrm{J} = 1 \rightarrow 0$ spectra of the 20 sources observed. We detected

[5]CLASS is part of the GILDAS software developed by IRAM.

TABLE 3

RESULTS ^{12}CS J $= 1 \rightarrow 0$

Source	T_{MB} (K)	V_{LSR} (km s^{-1})	Width (km s^{-1})	$\int T_{MB} dv$ (K km s^{-1})	Notes
VLA 1623	10.7(1.7)	3.82(0.04)	0.8(0.1)	9(1)	G
IRAS 16293−2422	9.3(1.7)	4.0(0.1)	1.8(0.2)	17(2)	G,F
M8 E	19.4(2.7)	10.83(0.06)	2.1(0.2)	44(3)	G
G9.62+0.19	16.2(0.8)	5.2(0.2)	37.9(0.4)	115(30)	BP,V
G10.47+0.03	10.6(1.3)	67.0(0.1)	8.4(0.3)	95(3)	BP,G,F
GGD 27	12.6(1.9)	12.69(0.06)	2.5(0.2)	34(2)	G
G20.08−0.14	4.2(0.7)	42.2(0.2)	6.2(0.4)	27(2)	G
G28.20−0.049	6.4(0.7)	95.7(0.4)	16.9(0.9)	64(12)	BP,F,V
G31.41+0.31	4.3(1.0)	96.4(0.3)	10.4(0.7)	48(7)	G,BW
IRAS 18566+0408	3.4(0.4)	84.2(0.4)	11.8(0.9)	18(5)	BP,MP,V
W51 e2/e8	20.7(1.7)	57.9(0.1)	11.4(0.3)	251(5)	4,BP,RW,G
IRAS 20126+4104	5.8(1.0)	−3.6(0.1)	3.0(0.3)	19(1)	G
S106IR	3.6(1.0)	−1.0(0.2)	1.4(0.5)	5.3(1.5)	BP,G
AFGL 2591	10.9(1.0)	−6.2(0.2)	7.7(0.4)	33(8)	BW,V
MWC 349	(1.2)	⋯	⋯	⋯	ND
W75N (B)	17.2(1.0)	9.5(0.1)	3.1(0.1)	57(2)	G
DR21 (OH)	28.2(1.8)	−3.8(0.2)	8.5(0.4)	104(15)	V
IC 1396N	6.6(0.9)	1.02(0.07)	2.1(0.2)	14(1)	BP,G
CEP A East	6.40(0.8)	−10.61(0.08)	4.1(0.2)	28(1)	BW,G
NGC 7538S	14.2(1.2)	−56.24(0.08)	4.8(0.2)	73(3)	G

NOTES: 1σ statistical errors from the fit are presented in parentheses. (MP) Multi-peak profile. (G) One Gaussian was used to fit the peak. In this case the width reported equals the FWHM of the line. (GMP) Overlapping Gaussians used to fit a multi-peak line profile. (V) Zero power width of a MP or asymmetric line is presented. The reported flux density and V_{LSR} correspond to the channel with greatest emission. The error presented in parenthesis for V_{LSR}, line width, and $\int T_{MB} dv$ are the channel width, twice the channel width, and the rms multiplied by the line width, respectively. (F) Possible 'flat-top' profile. (ND) Non-detection. (BW) Possible blue wing. (RW) Possible red wing. (BP) Non-flat bandpass shape may compromise line parameters.

TABLE 4

RESULTS ^{13}CS J $= 1 \rightarrow 0$

Source	T_{MB} (K)	V_{LSR} (km s^{-1})	Width (km s^{-1})	$\int T_{MB} dv$ (K km s^{-1})	Notes
M8 E	1.6(0.3)	10.7(0.1)	1.3(0.3)	2.3(0.4)	BP,G
W75N (B)	1.2(0.3)	9.2(0.5)	6.3(0.9)	3.3(0.1)	V
DR21 (OH)	0.9(0.2)	−2.8(0.3)	4.2(0.5)	3.9(0.5)	G

NOTES: Same as Table 3.

^{12}CS emission in 19 sources; the only non-detection is toward MWC 349 for which we report an upper limit on the main beam brightness temperature of 3.6 K (3σ). Ten of the detections have narrow lines (less then 5 km s^{-1} wide) and four of the sources show (possible) wing emission in their line profiles, suggesting that the CS J $= 1 \rightarrow 0$ transition may be tracing outflows in these regions. The source IRAS 18566+0408 shows a double peaked profile, with the blue peak being stronger than the red,
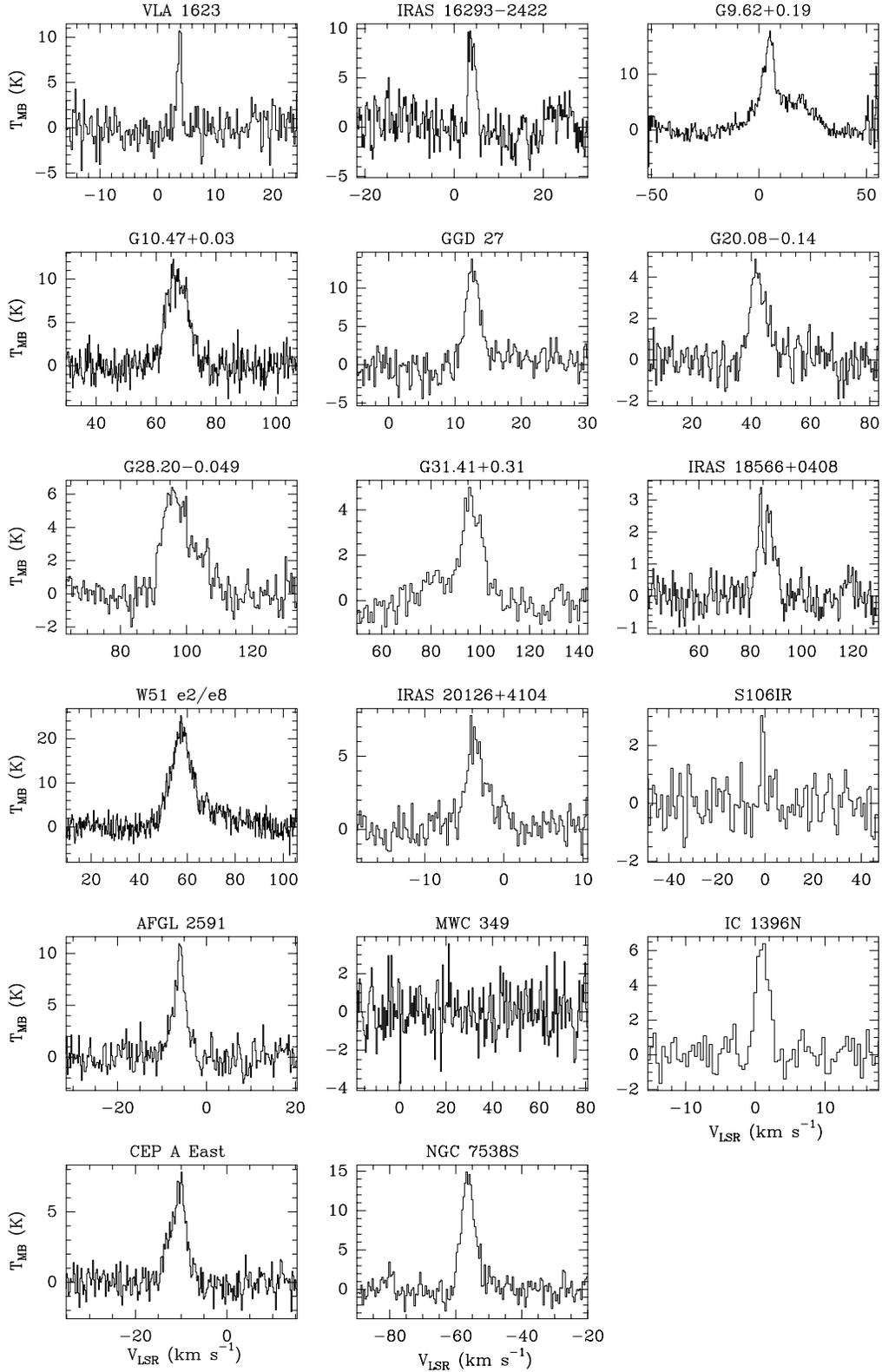
Fig. 1. Spectra of the 17 sources that were observed in the ^{12}CS J = 1 → 0 transition but not in ^{13}CS J = 1 → 0.

TABLE 5

RESULTS CH$_3$OH J$_K$ = 7$_0 \rightarrow$ 6$_1$ A$^+$

Source	S_ν (Jy)	V_{LSR} (km s^{-1})	Width (km s^{-1})	$\int S_\nu dv$ (Jy km s^{-1})	Notes
S235	104.4(5.4)	−16.41(0.01)	0.70(0.02)	77.2(2.0)	G,F
M8 E	1189.7(9.2)	10.84(0.04)	0.43(0.04)	543.3(4.8)	GMP
	493.3(9.2)	11.17(0.04)	0.23(0.04)	120.1(4.1)	
GGD 27	87.7(6.5)	12.21(0.01)	0.32(0.03)	29.2(2.0)	GMP
	263.5(6.5)	13.14(0.01)	0.63(0.01)	176.1(2.7)	
W51 e2/e8	69.0(4.8)	49.10(0.04)	0.63(0.04)	46.2(1.0)	GMP
	105.7(4.8)	49.40(0.04)	0.69(0.04)	77.9(1.0)	
	79.6(4.8)	50.30(0.04)	0.49(0.04)	41.5(1.0)	
	18.4(4.8)	54.66(0.04)	3.71(0.04)	72.4(1.0)	
	15.6(4.8)	56.30(0.04)	6.34(0.04)	106.1(1.0)	
DR21 (OH)	417.5(3.7)	0.01(0.02)	0.58(0.04)	255.3(20.4)	GMP
	469.5(3.7)	0.48(0.01)	0.40(0.02)	197.9(19.0)	

NOTES: For M8E the errors given for the width and the central velocity peak are the channel width. All notes are the same as Table 3.

TABLE 6

BEAM AVERAGED COLUMN DENSITIES

Source	log(N_{CS}) (cm^{-2})	log(N_{H_2}) (cm^{-2})
VLA 1623	14.2	22.5
IRAS 16293−2422	14.5	22.8
M8 E	14.9	23.1
G9.62+0.19	15.3	23.6
G10.47+0.03	15.2	23.5
GGD 27	14.8	23.0
G20.08−0.14	14.7	22.9
G28.20−0.049	15.0	23.3
G31.41+0.31	14.9	23.2
IRAS 18566+0408	14.5	22.8
W51 e2/e8	15.6	23.9
IRAS 20126+4104	14.5	22.8
S106IR	14.0	22.2
AFGL 2591	14.8	23.0
MWC 349	⋯	⋯
W75N (B)	15.0	23.3
DR21 (OH)	15.3	23.5
IC 1396N	14.4	22.7
CEP A East	14.7	23.0
NGC 7538S	15.1	23.4

NOTES: Column densities for the sources are calculated from the ^{12}CS data assuming optically thin emission. These are lower limits to the true column density. For the three sources for which we could determine the opacity of the ^{12}CS (1-0) line, we derive the corrected values quoted in § 4.2.

which could be a sign for the presence of infalling material.

We detected ^{13}CS J = 1 → 0 emission toward the three sources observed (see Figure 2). The ^{13}CS line toward M8 E is narrower than the corresponding ^{12}CS line, and the ^{13}CS line toward W75N (B) possibly has a second (red-shifted) component that is not observed in the ^{12}CS line profile. In the three sources observed, the ^{13}CS profiles show red asymmetries.

In Figure 3 we show the spectra of the CH$_3$OH 44 GHz maser observations. The brightest CH$_3$OH emission was found toward M8 E, and with the possible exception of S235, all sources show asymmetric and/or multi-peaked emission profiles, an indication of velocity superposition of different maser lines.

4. ANALYSIS AND DISCUSSION

4.1. *Beam Averaged Column Densities*

Assuming optically thin emission, we calculated beam averaged ^{12}CS column densities for each of the sources detected in the ^{12}CS line. We assumed that the gas is in LTE with a kinetic temperature of 20 K. We also estimated beam averaged total H$_2$ column densities from the CS column densities using a [^{12}CS]/[H$_2$] abundance ratio of 5.0×10^{-9} from Lapinov et al. (1998).

The beam averaged CS column densities are between 1 and 39.8 $\times 10^{14}$ cm^{-2}, and the H$_2$ column density values are between 1.6 and 79.4 $\times 10^{22}$ cm^{-2}. Our H$_2$ column density estimates agree on average within a factor of two with the values reported by Ikeda et al. (2001) for G31.41+0.31, G10.47+0.03, DR21 (OH), NGC 7538S, and W51 e2/e8. The beam averaged column densities are reported in Table 6.

TABLE 7

CS EXCITATION TEMPERATURE AND OPACITIES

Source	$[^{12}\text{C}]/[^{13}\text{C}]=36$			$[^{12}\text{C}]/[^{13}\text{C}]=53$			$[^{12}\text{C}]/[^{13}\text{C}]=66$		
	T_{ex} (K)	τ_0^{12}	τ_0^{13}	T_{ex} (K)	τ_0^{12}	τ_0^{13}	T_{ex} (K)	τ_0^{12}	τ_0^{13}
M8 E	23.6	3.0	0.08	22.8	4.6	0.09	22.6	5.8	0.09
W75N (B)	22.5	2.2	0.06	20.8	3.6	0.07	20.5	4.5	0.07
DR21 (OH)	133.3	0.2	0.007	44.8	1.1	0.02	37.6	1.7	0.03

NOTES: Excitation temperatures and opacities were estimated form the ^{12}CS and ^{13}CS data assuming LTE and smooth distribution of both emission lines through the beam. We calculated the excitation temperatures and opacities using three different $[^{12}\text{C}]/[^{13}\text{C}]$ isotopic ratios reported by Milam et al. (2005) toward DR21 (OH) that were obtained based on CN, CO and H₂CO observations.

4.2. *Excitation Temperature, Optical Thickness, and Column Densities based on the ^{13}CS and ^{12}CS Observations*

For the three sources observed in both ^{13}CS and ^{12}CS J = 1−0 lines, we calculate the excitation temperature and optical depth of the transitions assuming that the ^{13}CS and ^{12}CS emission trace the same gas. The solution of the radiative transfer equation including background radiation is (e.g., Stahler & Palla 2004):

$$T_{\text{B}_0} = T_0 \left[f(T_{\text{ex}}) - f(T_{\text{BG}})\right] \left[1 - \exp(-\Delta\tau_0)\right] \quad , \quad (1)$$

where $\Delta\tau_0$, T_{B_0} and T_{BG} are the optical depth, the measured brightness temperature at the line center and the brightness temperature of the background emission (2.7 K), respectively, and $f(T) \equiv [\exp(T_0/T) - 1]^{-1}$ where $T_0 = h\nu_0/k_B$, h is the Planck constant, and k_B is the Boltzmann constant. Assuming LTE, the excitation temperatures of the transitions are equal to the temperature of the gas. In addition, assuming that $\Delta\tau_0^{12}/\Delta\tau_0^{13} = [^{12}\text{C}]/[^{13}\text{C}]$, we can solve for the excitation temperature and optical depths of the two isotopomer transitions. In Table 7 we list the T_{ex} and $\Delta\tau$ values obtained for three different isotopic ratios reported by Milam et al. (2005).

We find that the ^{12}CS J = 1 → 0 transition is optically thick ($\Delta\tau_0 \gtrsim 1$) for the three sources, implying that the column densities derived under the optically thin approximation (Table 6) are lower limits. Based on the excitation temperature and optical depth estimates (Table 7) and following the formulation by Lapinov et al. (1998), we derive CS column density values of $\log(\text{N}_{CS})$ 15.5, 15.4, and 15.5 cm^{-2} for DR21 (OH), M8 E, and W75N (B) (assuming $[^{12}\text{C}]/[^{13}\text{C}] = 53$), respectively. These values are $\sim 40\%$ greater than the values obtained in the optically thin approximation (Table 6).

4.3. *CS J = 1 → 0 Emission as Distance Indicator*

Figure 4 shows the FWHM of the ^{12}CS J = 1 → 0 lines as a function of distance for all sources with ^{12}CS detection in our sample. We find a strong linear correlation between both variables with a best fit slope of $0.93 \, \text{km s}^{-1} \, \text{kpc}^{-1}$. This clear correlation ($r = 0.918$) agrees with Larson's Law, i.e., if the CS emission is more extended than the beam, then we expect wider line widths toward more distant objects because more turbulent gas would be included within the beam. This correlation suggests the possibility of using CS J = 1 → 0 line width measurements as a distance indicator for massive star forming regions in the Galaxy, possibly in conjunction with other commonly used techniques (e.g., Araya et al. 2002).

4.4. *Variability of the 44 GHz Methanol Masers*

Although the main purpose of observing CH₃OH 44 GHz masers in this project was to obtain pointing corrections, our observations allow us to compare the line profiles obtained in this work with previous single dish observations of the masers.

Haschick et al. (1990) report CH₃OH 44 GHz maser observations conducted with the Haystack telescope. We have three sources in common with the Haschick et al. (1990) sample: S235, W51, and DR21. In addition, the CH₃OH 44 GHz maser in GGD 27 was observed by Kalenskii et al. (1992) using the Yebes 14 m telescope with an antenna beam width of 2′, and the maser in M8E was observed by Slysh et al. (1994) with the Parkes telescope with a half power beam width of 1.6′. We detected clear evidence for variability in W51, GGD 27 and S235 based on changes in the line profile. Possible variability was also detected in DR21, and no significant change in the line profile was found in the case of the M8E maser although the absolute magnitude of the emission possibly changed. As an example of the variability found in the CH₃OH maser profiles, we
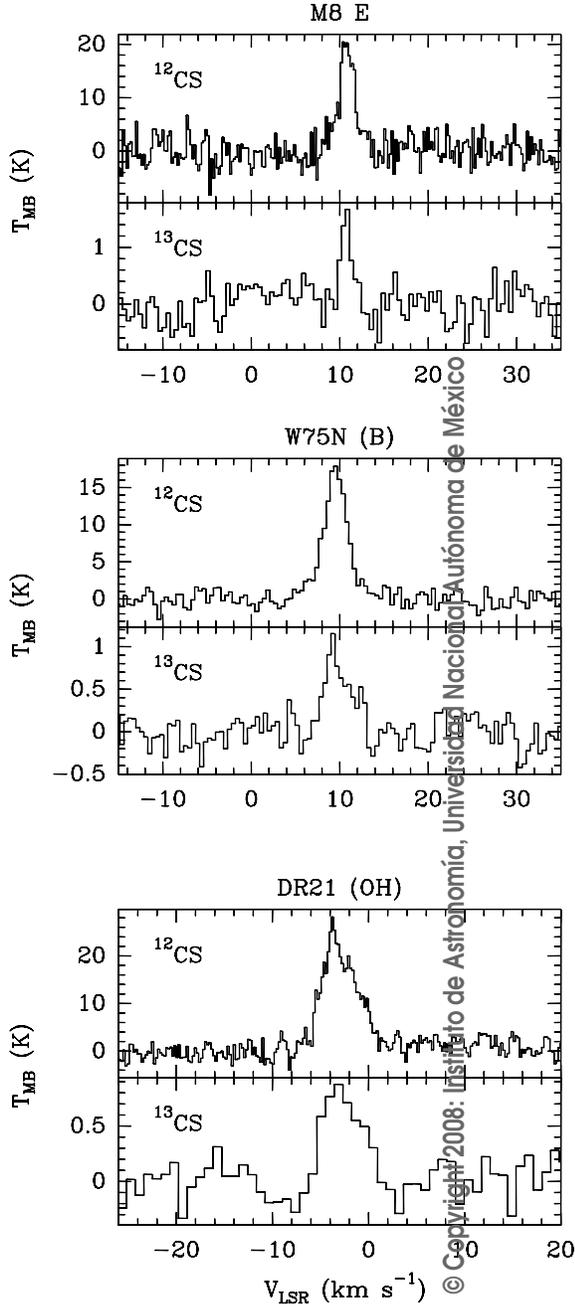
Fig. 2. Sources observed in both ^{12}CS (*upper panel*) and ^{13}CS J $= 1 \rightarrow 0$ transitions (*lower panel*).

present in Figure 5 the Haschick et al. (1990) spectrum (upper panel) and our spectrum of the CH$_3$OH 44 GHz masers in W51 e2/e8 (lower panel). Our observations show the occurrence of a strong and new CH$_3$OH emission feature redshifted by ~ 2 km s^{-1} from the velocity of the strongest maser component in W51 e2/e8.
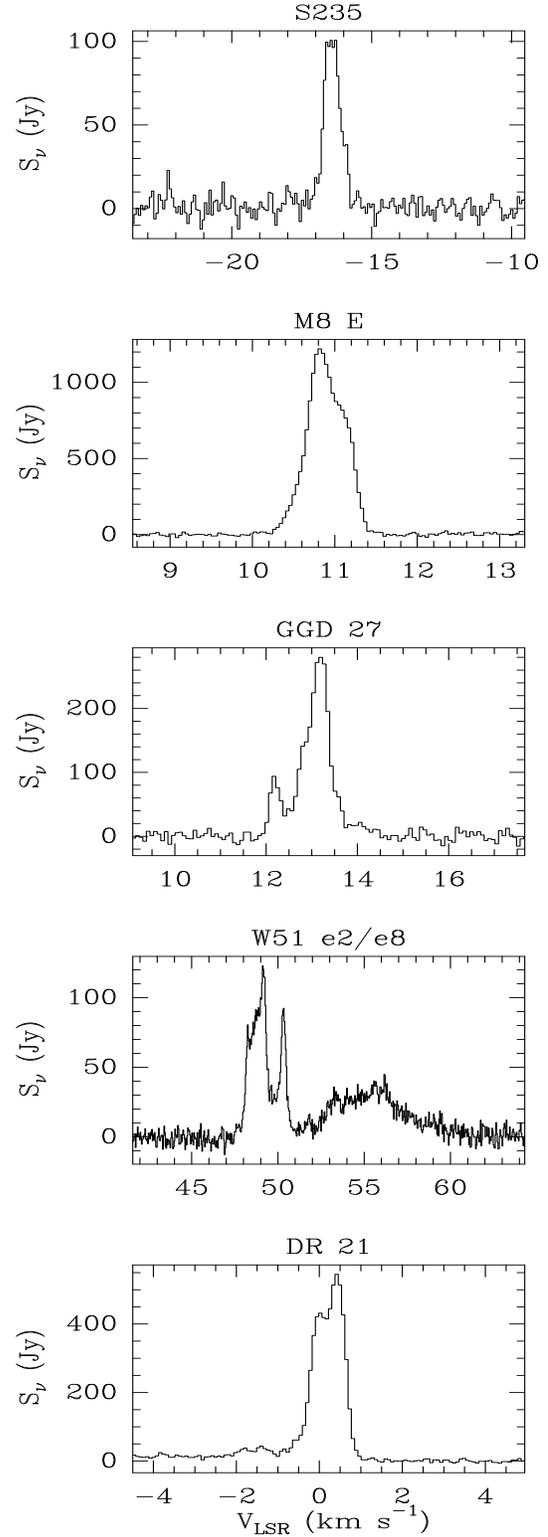
Fig. 3. CH$_3$OH J$_K = 7_0 \rightarrow 6_1$ A$^+$ spectra. We detected CH$_3$OH 44 GHz maser emission toward all five sources observed.
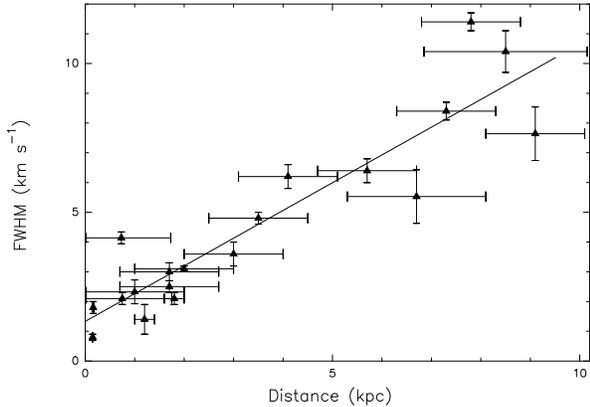
Fig. 4. FWHM of the ^{12}CS lines detected in this work as a function of the adopted distances to the sources. Our data show a strong correlation between line FWHM and distance with a slope of $0.93\,\mathrm{km\,s^{-1}\,kpc^{-1}}$.
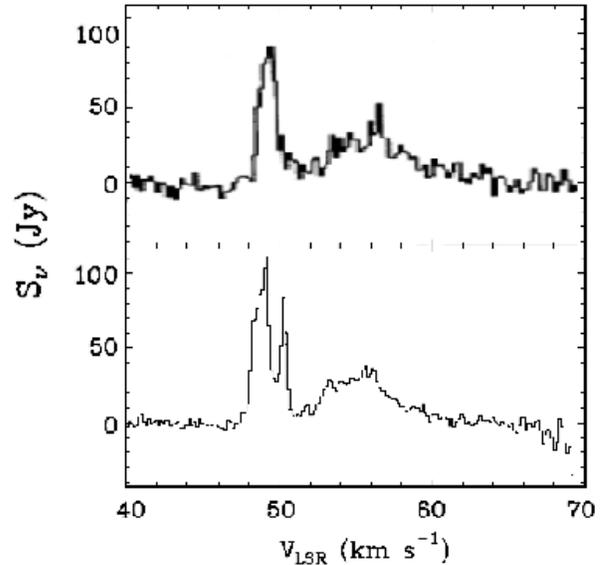

Fig. 5. Comparison of the 44 GHz CH$_3$OH masers in W51; the upper panel shows data from Haschick et al. (1990) obtained in 1988 with the 37 m Haystack telescope, the lower panel shows the spectrum from this work smoothed to approximately the same channel width of the Haschick et al. (1990) spectrum. A new, strong CH$_3$OH emission feature is present just redshifted from the peak maser. Note also the agreement in the flux density scale of both the main and the broad CH$_3$OH emission components, suggesting that there is no significant systematic error in the calibration of our data.

Despite the small number of sources observed in the CH$_3$OH 44 GHz line in this work, the high detection rate of variability based only on changes in the line profiles (i.e., without including absolute changes in the flux density) indicates that CH$_3$OH 44 GHz variability is a common phenomenon within time scales of several years (see also Kurtz et al. 2004). Finally, Figure 5 also shows that the flux density calibration is consistent with that of Haschick et al. (1990) within $\sim 20\%$, assuming that the brightest, and the broad emission components in the W51 e2/e8 spectra are not variable. This is not surprising for the latter, as it almost certainly represents thermal emission from the molecular hot cores in this region, whose emission lines have similar widths (see Haschick et al. 1990).

4.5. Detectability with the VLA

The Very Large Array (VLA) has Q-Band receivers capable of detecting ^{13}CS and ^{12}CS J = 1 → 0 emission. Given that we did not obtain maps, i.e., we do not know the extent of the CS emission, we cannot reliably determine the VLA integration time that would be required to detect the ^{13}CS and ^{12}CS J = 1 → 0 lines reported in this work. Nevertheless, we can explore the detection likelihood by using simple assumptions regarding the optical depth of the lines.

If the ^{12}CS emission were optically thick and coming from a gas in LTE at a temperature of 25 K, then the average extent of the ^{12}CS gas based on our detections would be on the order of 25″. A size of 25″ is approximately half the size of the most extended object that could be mapped with the VLA at

Q-Band[6], and the synthesized beam in the D configuration at Q-Band is $\sim 1.5''$. Thus, it would be quite challenging to detect the ^{12}CS emission because it would be substantially resolved over ~ 270 synthesized beams. We note that the emission is likely to be more extended than $25''\times25''$ given the strong correlation between FWHM and distance, which suggests that the ^{12}CS J = 1 → 0 emission fills the beam in all sources. Clearly, if the ^{13}CS emission were smoothly distributed over a $25''\times25''$ or larger area, then it would be even harder to detect since the emission is likely to be optically thin.

In the limiting case of ^{13}CS having optically thick emission from a Hot Molecular Core ($T_K \sim 100\,\mathrm{K}$), and based on the main beam brightness temperatures reported in Table 4, the size from where the emission would originate is of the order of $5''\times5''$ (or 3 synthesized beams of the VLA-D). Such emission would be easy to detect with the VLA given that the theoretical rms noise level achieved after one hour on

---

[6]VLA Status Summary, `http://www.vla.nrao.edu/astro/guides/vlas/current/node8.html`

source is $\sim 3\,\mathrm{K}$ (observing with 1 IF mode, 195 kHz channel width, and 27 antennas). In a more realistic case, the $^{13}\mathrm{CS}$ emission might not be optically thick, but still could be detectable with the VLA as long as the emission is contained within a few synthesized beams.

5. SUMMARY

Using the MIT Haystack 37 m antenna, we conducted observations of the $^{12}\mathrm{CS}$ $J = 1 \rightarrow 0$ transition toward 20 sources and detected emission in 19 of them. Three of the sources (M8 E, W75N (B), and DR21 (OH)) were also observed and detected in the $^{13}\mathrm{CS}$ $J = 1 \rightarrow 0$ transition. In addition, we observed the CH_3OH 44 GHz line toward 5 sources, primarily with the goal of using the CH_3OH 44 GHz masers to determine pointing corrections. Based on the line profile of the CH_3OH 44 GHz spectra, we found evidence for maser variability in 4 of the 5 sources observed, indicating that CH_3OH 44 GHz maser variability on time scales of several years is quite common.

We estimate lower limits of the CS and H_2 column densities based on the $^{12}\mathrm{CS}$ $J = 1 \rightarrow 0$ detections and assuming optically thin emission. The CS column density values are greater than $10^{14}\,\mathrm{cm}^{-2}$ and the H_2 column density values are $\gtrsim 10^{22}\,\mathrm{cm}^{-2}$.

We found a strong correlation between the FWHM of the $^{12}\mathrm{CS}$ $J = 1 \rightarrow 0$ lines and the heliocentric distance to the sources. This indicates that the $^{12}\mathrm{CS}$ emission is likely more extended than the Haystack beam, and that the velocity dispersion is greater in larger volumes of gas than in smaller volumes, just as expected from Larson's Law. The strong correlation found in this work suggests the potential use of $^{12}\mathrm{CS}$ $J = 1 \rightarrow 0$ emission as a tool to estimate distances to star forming regions throughout the Galaxy.

REFERENCES

Araya, E., Hofner, P., Churchwell, E., & Kurtz, S. 2002, ApJS, 138, 63

Araya, E., Hofner, P., Kurtz, S., & Bronfman, L. 2005a, ApJS, 157, 279

Araya, E., et al. 2005b, ApJ, 618, 339

André, P., Ward-Thomson, D., & Barsony, M. 1993, ApJ, 406, 122

Campbell, M. F., Hoffmann, W. F., Thronson, Jr., H. A., Niles, D., Nawfel, R., & Hawrylycz, M. 1982, ApJ, 261, 550

Downes, D., Wilson, T. L., Bieging, J., & Wink, J. 1980, A&AS, 40, 379

Edris, K. A., Fuller, G. A., Cohen, R. J., & Etoka, S. 2005, A&A, 434, 213

Evans, N. J. 1999, ARA&A, 37, 311

Felli, M., Massi, F., Navarrini, A., Neri, R., Cesaroni, R., & Jenness, T. 2004, A&A, 420, 553

Goetz, J. A., et al. 1998, ApJ, 504, 359

Haschick, A. D., Menten, K. M., & Baan, W. A. 1990, ApJ, 354, 556

Hofner, P., Kurtz, S., Churchwell, E., Walmsley, C. M., & Cesaroni, R. 1996, ApJ, 460, 359

Ikeda, M., Ohishi, M., Nummelin, A., Dickens, J. E., Bergman, P., Hjalmarson, Å., & Irvine, W. M. 2001, ApJ, 560, 792

Kalenskii, S. V., et al. 1992, Soviet Astron., 36, 517

Kurtz, S., Churchwell, E., & Wood, D. O. S. 1994, ApJS, 91, 659

Kurtz, S., Hofner, P., & Vargas, C. 2004, ApJS, 155, 149

Lapinov, A. V., Schilke, P., Juvela, M., & Zinchenko, I. I. 1998, A&A, 336, 1007

Leurini, S., Schilke, P., Wyrowski, F., & Menten, K. M. 2007, A&A, 466, 215

Lugo, J., Lizano, S., & Garay, G. 2004, ApJ, 614, 807

Martí, J., Rodríguez, L. F., & Reipurth, B. 1995, ApJ, 449, 184

Menten, K. M. 1991, ApJ, 380, L75

Milam, S. N., Savage, C., Brewster, M. A., Ziurys, L. M., & Wyckoff, S. 2005, ApJ, 634, 1126

Müller, H. S. P., Menten, K. M., & Mäder, H. 2004, A&A, 428, 1019

Noel, B., Joblin, C., Maillard, J. P., & Paumard, T. 2005, A&A, 436, 569

Pickett, H. M., Poynter, R. L., Cohen, E. A., Delitsky, M. L., Pearson, J. C., & Müller, H. S. P. 1998, J. Quant. Spectrosc. Radiat. Transfer, 60, 883

Reipurth, B., Armond, T., Raga, A., & Bally, J. 2003, ApJ, 593, 47

Shepherd, D. S., Kurtz, S. E., & Testi, L. 2004, ApJ, 601, 952

Shirley, Y. L., Evans II, N. J., Young, K. E., Knez, C., & Jaffe, D. T. 2003, ApJS, 149, 375

Slysh, V. I., Kalenskii, S. V., Val'tts, I. E., & Otrupcek, R. 1994, MNRAS, 268, 464

Stahler, S. W., & Palla, F. 2004, The Formation of Stars (Weinheim: Wiley-VCH)

Stark, R., et al. 2004, ApJ, 608, 341

Tafoya, D., Gómez, Y., & Rodríguez, L. F. 2004, ApJ, 610, 827

Thronson, H. A., Jr., & Harper, D. A. 1979, ApJ, 230, 133

Trinidad, M. A., et al. 2003, ApJ, 589, 386

Werner, M. W., Becklin, E. E., Gatley, I., Matthews, K., Neugebauer, G., & Wynn-Williams, C. G. 1979, MNRAS, 188, 463

Wood, D. O. S., & Churchwell, E. 1989, ApJS, 69, 831

Esteban Araya, Peter Hofner, Evan Jordan, and Mala Mateen: Physics Department, New Mexico Institute of Mining and Technology, 801 Leroy Place, Socorro, NM 87801, NRAO, P.O. Box 0, Socorro, NM 87801, New Mexico, USA (earaya,phofner@aoc.nrao.edu,ejordan,mmateen@nmt.edu).

Stan Kurtz: Centro de Radioatronomía y Astrofísica, Universidad Nacional Autónoma de México, Apdo. Postal 3-72, C.P. 58090 Morelia, Michoacán, Mexico (s.kurtz@astrosmo.unam.mx).